Proceedings of the 1984
Winter Simulation Conference
S. Sheppard, U. Pooch, D. Pegden (eds.)

COMPUTER EYE LOOKS AT HUMAN EYE

Bruce H. McCormick
Department of Computer Science
Texas A&M University
College Station, Texas 77843

Roland Priemer
Department of Electrical Engineering & Computer Science
University of Illinois at Chicago
Chicago, Illinois 60680

ABSTRACT

A television ophthalmoscope (TVO) developed at the University of Illinois at Chicago combines a low-light-level television camera and digital image processor to acquire and analyze images of the retina and choroid, one of the few areas of the body where the circulatory system can be observed in detail without surgery. So far the TVO has been used in two-wavelength oximetry to measure oxygen saturation in the blood--a measure useful in diagnosing and treating diabetes, with potential for better management of sickle-cell anemia, hypertension and other systemic diseases. The TVO image processor also analyzes multispectral reflectance images which have been used, for example, to calculate and display difference images of visual pigment density, related to night blindness and other inherited eye disorders. In addition, the use of the TVO in quantitative angiography has contributed to understanding of the dynamics of retinal/choroidal blood flow.

Experimental studies are presented that demonstrate two complementary techniques for the extraction of hemodynamic parameters from TVO-derived angiographic data. In particular both the frequency domain technique and the time domain technique presented are capable of obtaining retinal circulation time (RCT) estimates from nonuniformly sampled and noisy dye dilution curves. Both methods use identical input (artery dye dilution curve) and response (vein dye dilution curve). The frequency domain technique uses this information for obtaining transfer function estimates of the retinal capillary bed. These estimates are then used to obtain minimum mean square error values of parameters in a model of the capillary bed. The model was chosen so as to account for both the tracer transit time, which is the time the response is delayed relative to the input, and tracer dispersion, which is the extent to which the response pulse is spread out relative to the input pulse. This spreading effect is determined by the variation in capillary lengths within a capillary bed and by various types of mixing.

THE TELEVISION OPHTHALMOSCOPE

The television ophthalmoscope consists of a light source, camera, image processor and computer programs designed for image acquisition and analysis (Figure 1). In the TVO system, a fiber-optic system conveys light from a 300 W xenon arc source to the eye. On the way its light passes through a minicomputer-controlled wheel holding 17 narrowband (∿20 nm) interference filters that cover the visible spectrum (410-720 nm). A stepping-motor drive linked to the TVO's minicomputer rotates the filters, allowing the system to gather successive images in different spectral bands in 0.1 s, in sequences of up to 300 images.

Figure 1. An operator measures oxygen saturation in the blood--useful to diagnose and treat diabetes and other diseases--with the television ophthalmoscope (TVO).

The television camera is a special low-light-level silicon-intensified-target vidicon. The tv camera is mounted on a Zeiss fundus camera, a clinical instrument for photographing the ocular fundus, i.e., the back of the inside of the eyeball.

TV signals travel to the image processor, which was designed by A. Charles Petersen, senior research engineer at the University of Illinois at Chicago, Richard Borovec and McCormick. The image processor comprises a minicomputer with peripherals, an image memory and a special video controller. The memory

contains eight memory modules driven in parallel to give an effective word length of 128 bits with a maximum data rate of 171 Mbits/s. A fast scratchpad memory makes available both planar slices of an image and 8-bit gray scale values for 16 pixels, greatly speeding up image processing functions. The video controller is a high-speed digitizer which also provides for display and data management.

Over time, the TVO group has written 100 or so programs for special types of image sequence processing. For video angiography and other dynamic imagery, the software includes a "movie" facility that displays 20 frames per second. For high- resolution images, processing takes about 4 seconds per frame.

QUANTITATIVE ANGIOGRAPHY: GENERAL INTRODUCTION

Since blood flow can be observed directly through the retina with the TVO, the system is valuable for studying the dynamics of blood flow and blood volume. In both human beings and animal research, the method relies on measuring how quickly a harmless tracer dye circulates through the retina by measuring the fluorescence of dye in a retinal artery at a fixed location. Quantitative angiography of this type is a well-established procedure. However, previous methods were cumbersome, time-consuming, painful for unanesthetized subjects, and in practice were rarely performed. The TVO program compares a sequence of angiograms relatively rapidly, automatically adjusting for slight differences in light levels, eye motion and other changes. Given low light level and intravenous injection, the patient remains comfortable. With intravenous injection, of course, the dye travels to the heart, to the lungs, and back to the heart before reaching the retina. Since so much time elapses and the dye disperses, direct measurements can vary greatly from one run to another. Sidestepping this problem by time domain modeling, the time-domain TVO program breaks apart the observed dye dilution curve into components, each of which represents one pass of the tracer through the retinal circulation (Figure 2). The program picks an artery and a vein pair. After computing the dye dilution curves for a particular point in the artery and the vein, the program calculates the time it took the dye tracer to pass from the retinal artery into the vein.

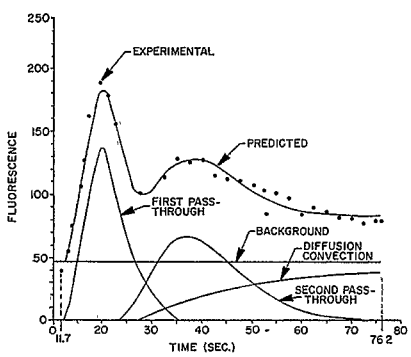

Figure 2. Dye dilution curve shows dynamics of blood flow in the human eye. Note excellent fit between model and experimental data processed by time-domain technique.

RETINAL CIRCULATION TIME AND VOLUME FLOW

Extraction of dye dilution curves

Retinal hemodynamic parameters have been measured in a series of twenty normal volunteers by the television ophthalmoscope using the indicator dilution technique of Zierler (1962). With the arm slightly elevated, a 0.1 ml pulse of 25% fluorescien was injected into the antecubital vein, followed immediately by a 3 ml saline flush. Two runs were made per subject, approximately fifteen minutes apart. After a short delay (the arm-retinal transit time) the fluorescein indicator appears in the retinal circulation, and the flow behavior of the retinal circulatory system can be examined with the television ophthalmoscope. Figures 3 and 4 show two out of a sequence of digitized fundus images. In Figure 3, arterioles are beginning to fluoresce as the tracer enters the retinal circulatory system. When the tracer leaves the retinal circulatory system, the retinal venules fluoresce, as shown in Figure 4. Note that these veins are barely visible in Figure 3.

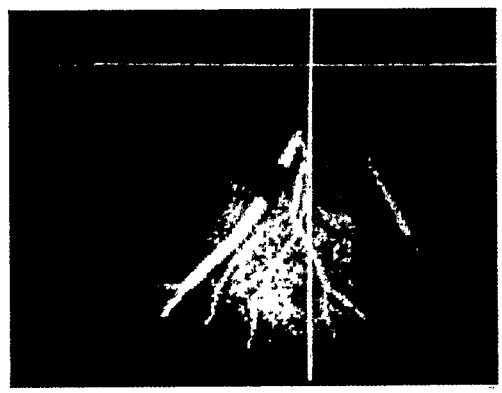

Figure 3. TVO Television Angiogram Frame: Early Arteriovenous Phase

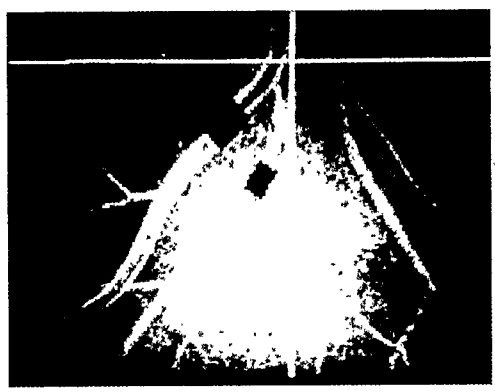

Figure 4. TVO Television Angiogram Frame: Slighty Later in Time Than Figure 3

Next, we select an associated artery-vein pair, within some unit area (such as those shown in Figures 3 and 4) and for each image the integrated fluorescence for the artery and vein is calculated. With these results, fluorescence versus time curves are shown in Figure 5. For a discussion of the preprocessing software see Read (1979). The work proposed here starts with data exemplified by Figure 5.

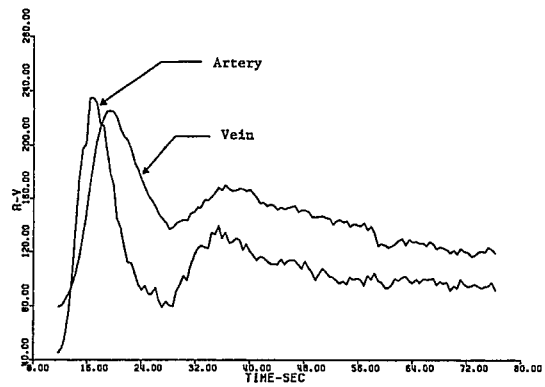

Figure 5. Raw Dye Dilution Data, Subject R4

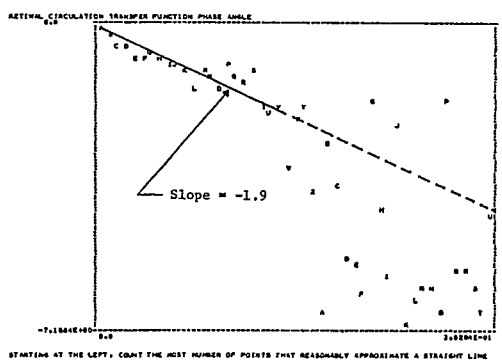

Figure 6. Subject R4, RCT = 1.9 seconds

Extraction of Hemodynamic Parameters: Retinal Circulation Time (RCT)

The computer-based system described above can quickly generate dye dilution curves. From these curves let us determine the blood transit time through various sectors of the retinal circulatory system.

Let $a_o(t)$ and $v_o(t)$ represent the artery and vein dye dilution functions respectively for a single pass-through of the tracer. To determine the tracer circulation time, consider first some function x(t), which is zero for t<0. The time centroid T(x) of x(t) is given by

$$T(x) = \int tx(t)dt \,/\, \int x(t)dt \qquad (1)$$

where x(t) is such that both integrals are finite and the denominator is not zero. A commonly accepted measure (Grodins, 1962) of the tracer circulation time T_R is

$$T_R = T(v_o) - T(a_o) \qquad (2)$$

In practice, there are many difficulties in implementing equation (2); we found poor agreement between the first and second runs with the same patient. We attribute this to nonreproducibility in the delivery of the dye bolus to the right atrium and to distortion of the down slopes of the dye dilution curves by recirculation when the dye bolus was too dispersed. The usual method of computing retinal circulation time (RCT) depends on reliable removal of recirculation effects from both arterial and venous curves. The calculation of RCT is sensitive to changes in the time constant of the descending limb, so any error in recirculation removal can have severe effect on the RCT.

We have developed programs to perform a frequency-domain analysis of the dilution curve data (Priemer, 1979). This algorithm produces an estimate of RCT which does not depend on removing recirculation effects. The circulatory segment between artery and vein is modeled as a linear system, with the arterial curve as input and the venous curve as output. The rate of change in phase as a function of frequency estimates the average dye transit time, or RCT. Preliminary experiments with this procedure have demonstrated significant improvement in RCT reproducibility.

In general our experience with careful and repeated acquisition, digital filtering, and modeling of human retinal dye dilution curves leads us to place only limited credence on the published clinical literature of retinal circulation times--both in the time distributions of RCT reported and because of the sampling bias introduced by methods applicable only to patients with exceptional powers of fixation.

The dititized image sequence provided by the television ophthalmoscope also allows a unique opportunity: the simulataneous extraction of dye dilution curves from all segments of the retinal circulation. Modeling techniques to measure the partitioning of blood among the competing circulatory segments is a specific research aim also discussed below.

ANALYSIS OF DYE DILUTION CURVES

Frequency Domain Technique

A segment of the retinal circulatory system is shown in Figure 7a. Here it is assumed that this segment is not coupled to other capillary beds. The functions a(t) and v(t) are the dye dilution curves, and the relationship between these two functions does not depend on how the tracer is injected or even on tracer recirculation. Instead, given that the fluidic nature of blood remains constant, tracer transit time (RCT) depends on the physical characteristics of the retinal vasculature.

This vasculature is modeled in Figure 7b, where a(t)

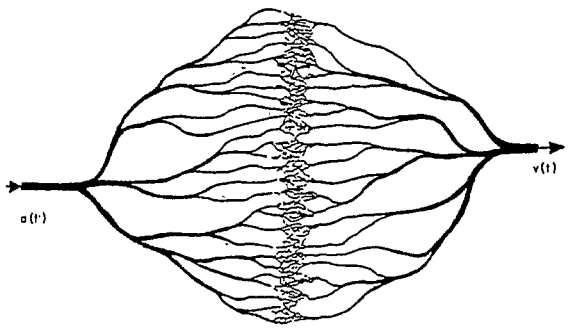

Figure 7a. Representation for a Single Segment Retinal Circulation (Artery-Vein Pair)

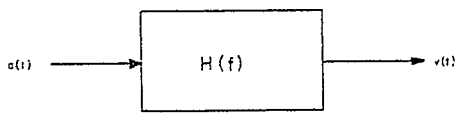

Figure 7b. Linear System Model of Retina Segment Circulation

is the input to some linear time-invariant system with transfer function H(f), and v(t) is the the response. If v(t) is simply a delayed version of a(t), then

$$v(t) = a(t - T_R) \qquad H(f) = e^{-j2\pi f T_R} \tag{3}$$

and the angle of H(f) is a linear function of frequency, the slope of which is the tracer transit time, i.e., $\angle H = -T_R (2\pi f)$. This is the basis of the method described here for finding the RCT.

From dye dilution curves such as in Figure 5, it can be seen that v(t) is not only a delayed version of a(t), but is also a spread out version of a(t). This is due in part to diffusion and convection of the tracer within the capillary bed. Also, this spreading is caused by variations in capillary lengths, which may be the dominant factor in the spreading effect. It is likely that some measure of this spreading effect is a significant physiological parameter. The form for H(f) in equation (3) cannot account for this spreading effect.

The Fourier transform pair for any function x(t) is given by

$$X(f) = \int_{-\infty}^{\infty} x(t)e^{-2j\pi ft}dt \qquad x(t) = \int_{-\infty}^{\infty} X(f)e^{j2\pi ft}df \tag{4}$$

or $X(f) = F(x(t))$ and $x(t) = F^{-1}(X(f))$. Let $A(f) = F(a(t))$ and $V(f) = F(v(t))$, and therefore

$$V(f) = H(f)A(f) \tag{5a}$$

$$v(t) = \int_{-\infty}^{\infty} h(t - \tau)a(\tau)d\tau = h(t) * a(t) \tag{5b}$$

where $h(t) = F^{-1}(H(f))$ and is called the impulse response of the system. In terms of magnitudes and phase angles, equation (5a) can be written as

$$||V(f)|| = ||H(f)||\ ||A(f)|| \tag{6a}$$

$$\angle V(f) = \angle H(f) + \angle A(f) \tag{6b}$$

The raw data $a(t_i)$ and $v(t_i)$ are used to obtain estimates of $\angle H(f)$ and $||H(f)||$. If $\angle H(f)$ versus f turns out to be a straight line, then T_R is the slope of the line, which can easily be calculated. Unfortunately, $a(t_i)$ and $v(t_i)$ are nonuniformly sampled and noisy data. Therefore, estimating $\angle H(f)$ and $||H(f)||$ is not a straightforward task.

Suppose, in consideration of Figure 7, that if a(t) is a short pulse, then v(t) is a Gaussian-like curve. This implies that capillary lengths are Gaussian distributed (assuming that other physical characteristics are the same) and therefore

$$h(t) = \frac{K}{\sigma\sqrt{2\pi}} e^{-\frac{(t-m)^2}{2\sigma^2}} \tag{7}$$

where m is the mean value, σ is the standard deviation, and K is some scale factor. Therefore σ^2 is a measure of the variance about the average length of capillary lengths. Now the transfer function is given by

$$H(f) = K\, e^{-jm2\pi f} e^{-\frac{\sigma^2}{2}(2\pi f)^2} \tag{8}$$

and therefore the angle of H(f) is still a linear function, while the magnitude of H(f) is also a Gaussian form, i.e.,

$$\angle H(f) = -m2\pi f = \angle V(f) - \angle A(f) \triangleq -\theta(f) \tag{9}$$

The choice for h(t) in equation (7) has resulted in a particularly straightforward method for obtaining the RCT = T_R = m, which is the slope of a straight line fitted to $\theta(f)$.

Now estimates V_k and A_k of V(f) and A(f) at $f = f_k$, k = o,..., L - 1 must be obtained so that

$$\angle H(f_k) = \angle V_k - \angle A_k \tag{10a}$$

$$||H(f_k)|| = ||V_k||/||A_k|| \tag{10b}$$

versus frequency $f = f_k$ can be computed. The optimum slope m of a straight line can be found by minimizing the mean square error between the form in equation (9) and the data in equation (10a). Similarly, an estimate for σ^2 can be obtained by fitting the data in equation (10b) to the Gaussian form in equation (8). The details of this are given in (Priemer, 1979). In equation (10b), a division is necessary, and this causes estimates of $||H(f)||$ to be erratic.

For the purposes of numerically obtaining a Fourier transform with a useful frequency resolution, the f_k are given by $f_k = k(1/T_0)$, where T_0 is the duration of the time function being Fourier transformed. Typically, the duration of a dye dilution curve is too short. If the transients have decayed, then the raw

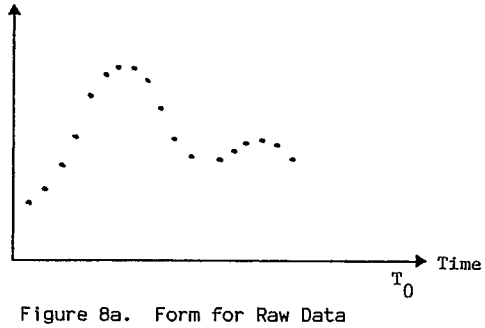

Figure 8a. Form for Raw Data

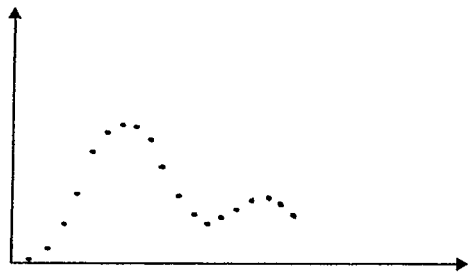

Figure 8b. Translated Data

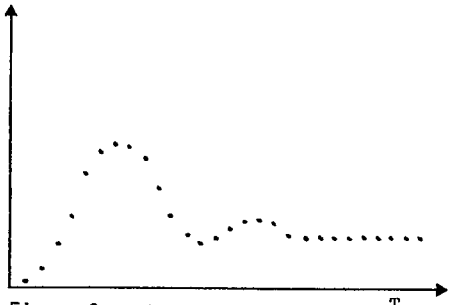

Figure 8c. Augmented Data

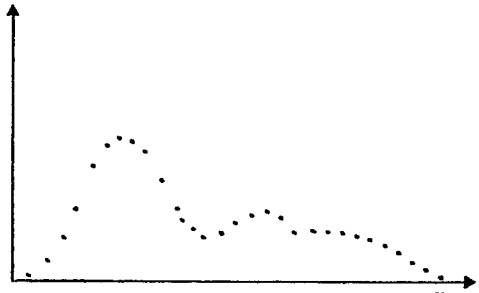

Figure 8d. Windowed Data

data can be translated and augmented to achieve a sufficiently large T_0. The data must further be windowed to reduce ripple error in the Fourier transform. These data preparation steps are illustrated in Figure 8.

Since the data is not uniformly sampled, a typical FFT algorithm cannot be used. Instead, the Fourier transform $A(f_k)$ is obtained with the trapezoidal rule for numerical integration, which is

$$A(f_k) = \sum_{i=0}^{N-1} \frac{1}{2}(a(t_i)e^{-j2\pi f_k t_i} + a(t_{i+1})\, e^{-j2\pi f_k t_{i+1}})(t_{i+1} - t_i) \qquad (11)$$

where N is now the total number points in the duration T_0. In a similar manner $V(f_k)$ is obtained.

The utility of the approach for estimating the RCT that has been presented here can now be illustrated. In Figure 9 are dye dilution curves for subject R1. These curves possess several desirable characteristics, which are : (1) the transients have decayed out, (2) there is a clear first and second tracer pass-through and perhaps even a third pass-through, and (3) the curves are relatively smooth and noise free. Figure 10 shows $\angle H(f_k)$ versus f_k, and a solid line was drawn to approximate the plot within the bandwidth of the data. The data points reasonably follow a straight line, the slope of which yields RCT = 1.8 seconds. For the same subject and artery/vein pair, another dye dilution curve set (shown in Figure 11) was obtained. The RCT turned out to be 1.6 seconds. Within the bandwidth of the dye dilution curves, the data points in Figure 12 again follow a straight line, and the RCT appears to be reproducible.

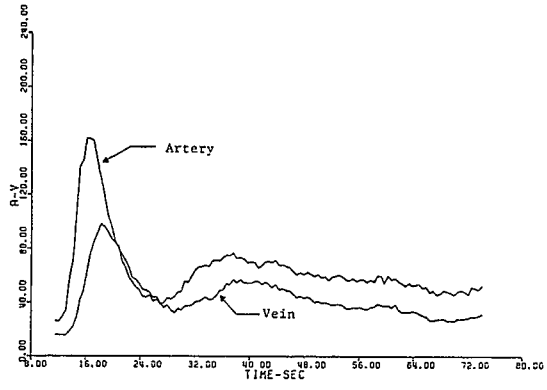

Figure 9. Raw Dye Dilution Data, Subject R1a

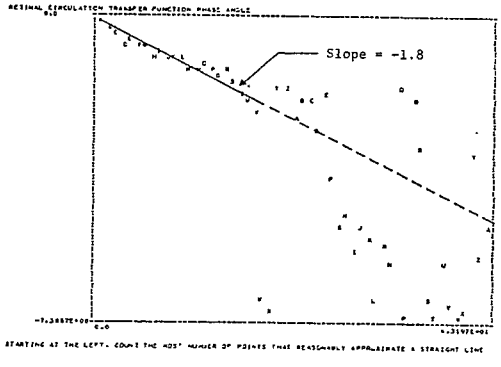

Figure 10. Subject R1a, RCT = 1.8 seconds

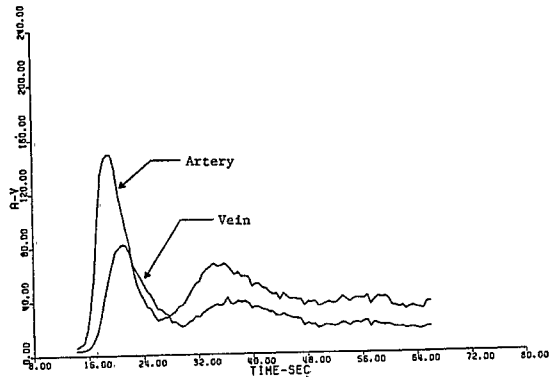

Figure 11. Raw Dye Dilution Data, Subject R1b

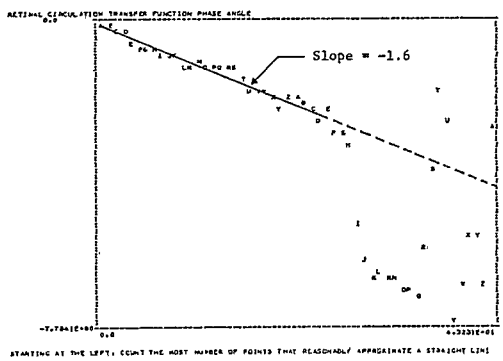

Figure 12. Subject R1b, RCT = 1.6 seconds

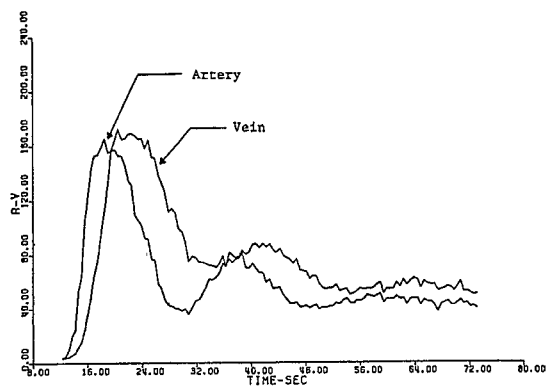

Figure 13. Raw Dye Dilution Data, Subject R2a

For another subject, dye dilution curves are shown in Figures 13 and 15, and the phase angle estimates yield the similar RCT values of 2.4 seconds and 2.2 seconds. For the same subject, but another artery/vein pair, the dye dilution curves do not possess the desirable characteristics mentioned earlier, and the consequence of this is that a clear straight line approximation is not apparent.

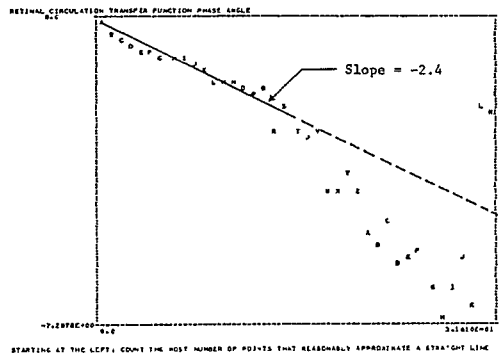

Figure 14. Subject R2a, RCT = 2.4 seconds

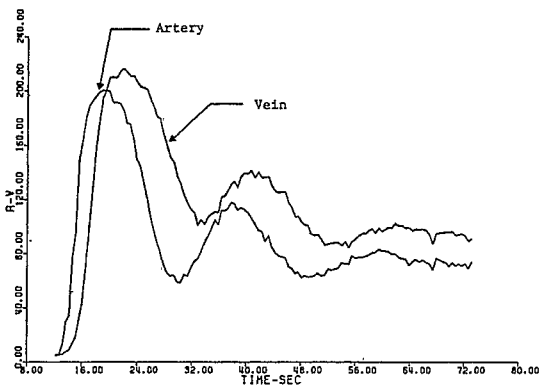

Figure 15. Raw Dye Dilution Data, Subject R2b

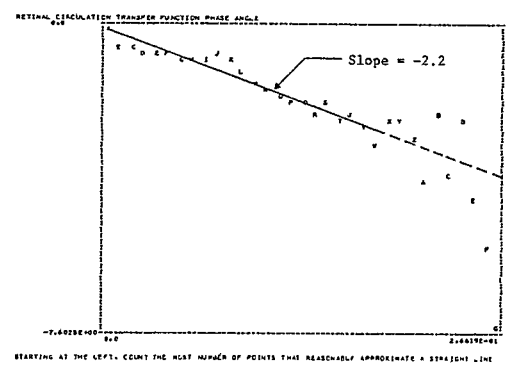

Figure 16. Subject R2b, RCT = 2.2 seconds

Time Domain Method

Again let $a_o(t)$ and $v_o(t)$ represent the artery and vein dye dilution functions respectively for a once pass through of the tracer. A time domain technique will be described, with which models for $a_o(t)$ and

$v_o(t)$ can be extracted from the actual retinal tracer dilution functions $a_R(t)$ and $v_R(t)$ respectively. The derived once-pass-through functions can then be used to compute the retinal circulation time, as described above.

Circulation through the heart has been indicated as one cause for tracer recirculation components in the retinal dye dilution curves. Therefore, $a_o(t)$ and $v_o(t)$ cannot be directly obtained. Instead, data related to $a_R(t)$ and $v_R(t)$ as given by

$$a_R(t) = a_o(t) + a_1(t) + \dots + a_I(t) + d_a(t) \quad (12a)$$

$$v_R(t) = v_o(t) + v_1(t) + \dots + v_I(t) + d_v(t) \quad (12b)$$

can be accessed, where $a_i(t)$ and $v_i(t)$, $i=1, \dots, I$ are recirculation components, and $d_a(t)$ and $d_v(t)$ are steady state convection-diffusion components. The transition to a thoroughly mixed tracer, i.e. constant concentration, is nebulous, and therefore I is also unknown. The data that can be obtained is represented by

$$a(t_i) = a_R(t_i) + n_a(t_i) \quad (13a)$$

$$v(t_i) = v_R(t_i) + n_v(t_i) \quad (13b)$$

for $i = 0, \dots M-1$, where n_a and n_v are measurement noise. The time points t_i cannot be assumed to be uniformly spaced, which as will be seen in the sequel presents some numerical difficulties. Further, to prevent retinal radiation damage due to the illumination levels required for image acquisition, it is desirable to minimize M. These various difficulties unfortunately complicate the development of computer algorithms for directly calculating parameters such as T_R from data modeled by equation (13).

We now describe a method for separating the components $a_i(t)$, $d_a(t)$, $v_i(t)$, and $d_v(t)$, $i = 0,\dots, I$ in $a_R(t)$ and $v_R(t)$. After functional forms for $a_o(t)$ and $v_o(t)$, which are the once-through dye dilution functions have been obtained, then T_R can be computed with equation (2).

An inspection of plots such as those shown in Figure 5 reveals that a useful model for $a_o(t)$ is

$$a_o(t) = c_1 t^{c_2} \exp(-(c_3 t^2 + c_4 t))u(t) \quad (14)$$

where the dye dilution curve start time has been referenced to $t = 0$ with the unit step function, and similarly for $v_o(t)$. For some assignment to the parameters $c_1, \dots, c_4$, a sketch of $a_o(t)$ is shown in Figure 17. Further, it is assumed that the recirculation components are time-shifted functions having the same form as the first pass-through components. Finally, the convection-diffusion component is represented by an error function, which describes the physical behavior of the diffusion process. Then, for example, with $I = 1$, $v_R(t)$ is modeled by

$$v_R(t) = V_1 + V_3 \operatorname{erf}(V_4(t-V_2))u(t-V_2) + V_6(t-V_5)^{V_7} \exp(-(V_8(t-V_5)^2 + V_9(t-V_5)))u(t-V_5) + V_{11}(t-V_{10})^{V_{12}} \exp(-(V_{13}(t-V_{10})^2 + V_{14}(t-V_{10})))u(t-V_{10}) \quad (15)$$

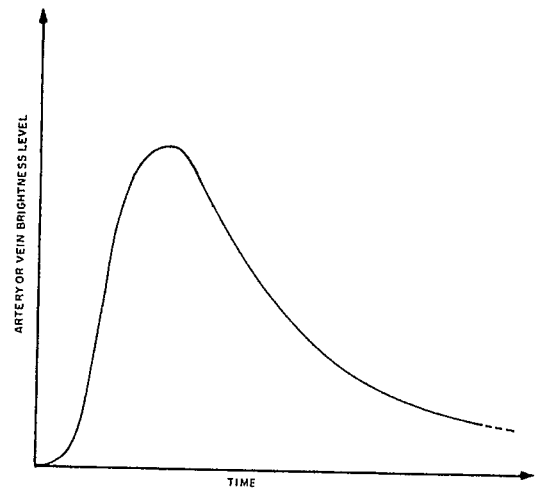

Figure 17. Time Domain Model: One Pass Through Dye Dilution Curve Model

or $v_R(t) = v_R(V,t)$, which is a function of time and the parameter set $V = (V_1, \dots, V_{14})$. Similarly, $a_R(t) = a_R(A,t)$, where A is the parameter set $A = (A_1, \dots, A_{14})$. Note, the parameters A_i and V_i, $i = 5, \dots, 9$ define the a_o and v_o components, while for a_1 and v_1, $i = 10, \dots, 14$. Hereafter, the dye dilution curves in Figures 18 and 19 will be used so that reference to a specific example can be made.

For $a_R(t)$ the parameters A are determined by minimizing the sum $e_a(A)$ of the errors squared in fitting the data, where $e_a(A)$ is given by

$$e_a(A) = \sum_{i=0}^{M-1} W_i(a_R(A, t_i) - a(t_i))^2 \quad (16)$$

The W_i are weightings, which can be preassigned in order to emphasize any particular data points. For $v_R(t)$, $e_v(V)$ is similarly defined. Normally, $W_i = 1$, and I is determined by inspection of the dye dilution curves. For Figures 18 and 19 I= 1 is a reasonable choice.

The method for minimizing each e is related to the simplex method, and does not require the calculation of any derivatives. Instead, only repeated evaluation of the function being minimized is necessary in this method. Therefore, the forms chosen for $a_R(t)$ and $v_R(t)$ can be any functions deemed to be suitable for fitting the data. The mechanism by which the minimization procedure operates is beyond the scope of this paper. However, as for any function minimization technique, useful results can be more readily obtained if a good initial guess is provided for the independent variables. Also, it is preferable that

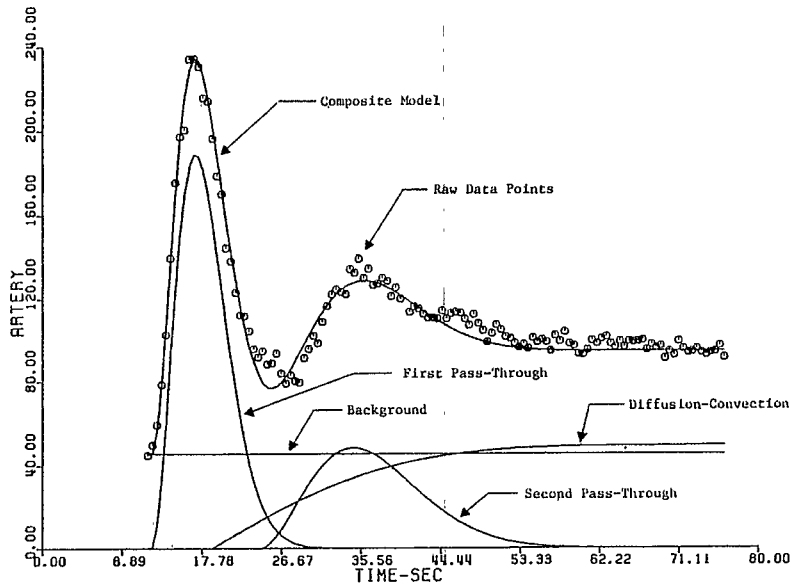

Figure 18. Decomposition of Dye Dilution (Artery) for Subject R3

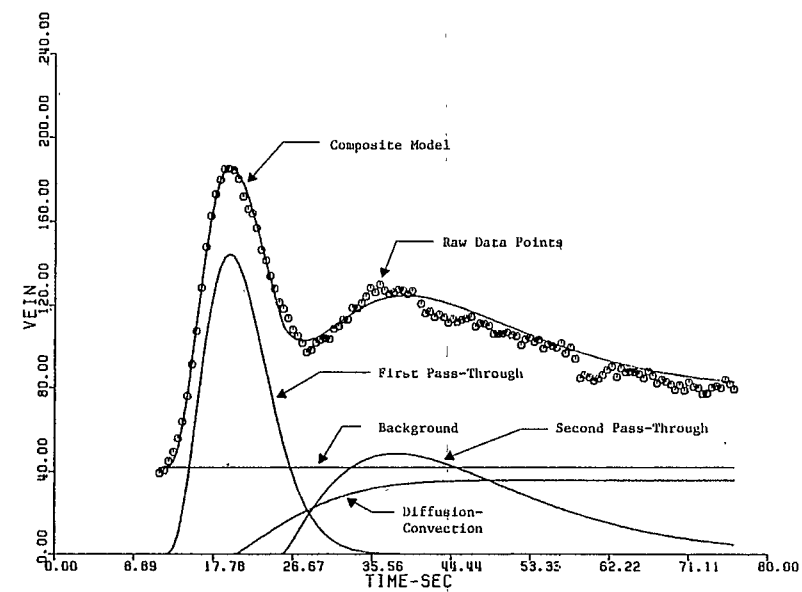

Figure 19. Decomposition of Dye Dilution (Vein) for Subject R3

the initial guess be data dependent so that its computation can also be automated.

The initial guess is computed based on the form chosen for the dye dilution function. The time t_o is the initial time, and $a(t_o)$ is the initial value. Let t_{max} denote the time when the experimental data $a(t_i)$ takes on its maximum value with respect to t. An initial guess can now be assigned to some of the parameters, i.e.

$$A_1 = a(t_o)$$

$$A_2 = t_o \qquad (17)$$

$$A_3 = a(t_{M-1}) - a(t_o)$$

$$A_4 = 1.0/(8t_{max})$$

The choice for A_4 ensures that the error function does not approach the value 1.0 until a time significantly greater than t_{max}. The initial guess for the parameters in a was chosen so that $a_o(t_{max}) = a(t_{max})$, and therefore

$$\begin{aligned} A_5 &= t_o \\ A_6 &= e^{3/2}\,(a(t_{max}) - a(t_o))/t^2_{max} \\ A_7 &= 2.0 \\ A_8 &= 1.0/(2t^2_{max}) \\ A_9 &= 1.0/t_{max} \end{aligned} \tag{18}$$

The next term was initially specified to start at $t = t_{max}$ with a peak value down by the factor e^2, and therefore

$$\begin{aligned} A_{10} &= t_{max} \\ A_{11} &= A_6/e^2 \\ A_{12} &= 2.0 \\ A_{13} &= A_8/4 \\ A_{14} &= A_9/2 \end{aligned} \tag{19}$$

In a similar manner the initial guess for V was obtained. Of course, these parameters will be optimized to achieve at least a local minimum in the sum of the errors squared functions $e_a(A)$ and $e_v(V)$. (Priemer, 1979) gives the program listing (written in FORTRAN) that implements all of the above.

From the output, Figures 18 (artery) and 19 (vein) were obtained. These plots indicate that this approach can yield good over-all models. Further, the use of $a_o(t)$ and $v_o(t)$ shown results in $T_R = 3.1$ seconds.

In order to assess the utility of the above described technique there are some shortcomings that cannot be ignored. The complexity of e_a or e_v precludes the knowledge of whether or not a global minimum can be achieved. The minimization method is an iterative scheme that fits the over-all data to a model, and therefore a small variation in e_a and e_v can cause a large variation in the components a_o and v_o. Consequently, the use of equation (2) for T_R is very sensitive to the number of iterations and the initial guess for parameters. Obviously, the forms chosen for a_R, a_o, v_R, and v_o influence T_R. Finally, no relationship between a_R and v_R was incorporated in the models.

However, the main advantages (i.e. noise immunity, tolerance for missing data, and facility for trying any functional forms in a_R and v_R) of this technique do allow for easily using this technique to evolve new models.

Also, since the resulting models are smooth continuous functions, further analyses, such as spectral analysis, can more readily be performed.

Circulation Interaction Between Retinal Segments

To this point circulation interaction between retinal segments has not been considered. Now however, the TVO facility has evolved so that dye dilution curves for all major retinal arteries and veins can be simultaneously obtained. This will allow investigation of the entire retinal circulation system as is represented in Figure 20 where $a^1(t)$ and $v^1(t)$ are dye dilution curves.

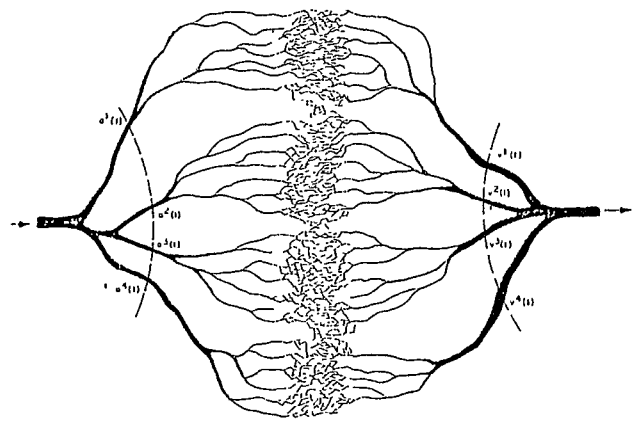

Figure 20. Representation of a Multiple Segment Retinal Capillary Bed

To extend the model of Figure 20, let

$$A(f) = \begin{bmatrix} F(a^1(t)) \\ F(a^2(t)) \\ \cdot \\ \cdot \\ \cdot \\ \cdot \end{bmatrix} \quad \text{and} \quad V(f) = \begin{bmatrix} F(v^1(t)) \\ F(v^2(t)) \\ \cdot \\ \cdot \\ \cdot \\ \cdot \end{bmatrix} \tag{20}$$

and therefore

$$V(f) = \begin{bmatrix} H_{11}(f) & H_{12}(f) & \cdots \\ H_{21}(f) & H_{22}(f) & \\ \cdot & \cdot & \\ \cdot & \cdot & \\ \cdot & & \cdot \end{bmatrix} A(f) \tag{21}$$

or $V(f) = H(f)A(f)$, where $H(f)$ is now a transfer function matrix. For each $H_{ij}(f)$, a form as in equation (8) could be assumed, and therefore each entry in H(f) involves the unknown parameters K_{ij}, m_{ij} and σ_{ij}, which must be estimated based on $V(f_k)$ and $A(f_k)$, $k = 0, \ldots, L-1$.

In addition to these frequency domain results, cross-

correlation estimates are also useful for assessing the extent to which different retinal capillary beds interact. By equation (21), $v^i(t)$ is given by

$$v^i(t) = h_{i1}(t) * a^1(t) + \ldots + h_{ii}(t) * a^i(t) + \ldots \quad (22)$$

The cross-correlation $r_{ij}(u)$ of $v^i(t)$ and $a^j(t)$ is given by

$$r_{ij}(u) = \int a^j(t-u)v^i(t)dt = a^j(-u) * v^i(u) \quad (23)$$

where u is the time displacement of $a^j(t)$ relative to $v^i(t)$.

Dye dilution curves for the arteries and veins shown in Figure 20 were obtained and analyzed according to the methods described above. The results are summarized in the following table, where three tracer injections were given. Overall, these resulting dye dilution curves did not possess the desirable characteristics that were described in the previous section. The transients in B1, C1-C4 do not decay. However, the RCT $\approx$ 0 seconds in C3 is reasonable for the vessel pair v_2/v_1, and the small RCT in C2 is reproduced in C7 for the vessel pair a_3/v_5.

These results clearly show the need for an interactive analysis system. In such a system, an operator would edit out inconsistent data points and truncate dye dilution curves. For example, the data for C9a is noisy, and the transients have not decayed. A visual inspection would result in data truncated at approximately t = 24 seconds. The resulting phase angle plot will certainly be an improvement of the plot used in estimating C9b. A visual inspection by an operator would quickly determine the suitability of data and results and any further appropriate data preparation steps.

RCT Estimates for Figure 20

Figure	Injection	Upstream Vessel	Downstream Vessel	RCT (seconds)
B1	1	a_2^1	v_4^3	1.5
C1	1	a_3	v_5	1.6
C2	1	a_2	v_1	0.9
C3	1	v_1	v_2	---
C4	1	a_1	v_2	1.1
C5	2	a_2^1	v_4^3	2.2
C6	2	a_3	v_5	1.8
C7	2	a_2	v_1	0.6
C8	2	v_1	v_2	---
C9	2	a_1	v_2	---
C10	3	a_2^1	v_3^2	2.3
C11	3	a_2	v_3	1.7 - 4.5
C12	3	a_3	v_4	2.1
C13	3	v_5	v_1	---

CONCLUSION

Extensive experimental results have been presented in this paper to demonstrate two techniques for obtaining RCT estimates from nonuniformly sampled and noisy dye dilution curves.

The frequency domain technique uses the input (artery dye dilution curve) and response (vein dye dilution curve) for obtaining transfer function estimates of the retinal capillary bed. These estimates are then used to obtain minimum mean square error values of parameters in a model, which was developed here, of the capillary bed. The model was chosen so as to account for both the tracer transit time, which is the time the response is delayed relative to the input, and tracer dispersion, which is the extent to which the response pulse is spread out relative to the input pulse. This spreading effect is determined by the variation in capillary lengths within a bed and various types of mixing.

The phase angle of the transfer function model is a linear function of frequency, the slope of which is the tracer transit time. As can be seen in the many figures included in this report, the data (dye dilution curves) yielded transfer function phase angle estimates, which are also linearly dependent on frequency. By fitting a straight line to the phase angle estimates, the RCT can be determined. Due to noise contributions in the dye dilution data, only low frequency phase angle points were used for a straight line fit. Over-all, it has been demonstrated here that the phase angle data is indeed linear and that reproducible RCT estimates can be obtained.

Results for estimating σ, which is a measure of the spreading effect, in equation (7) are not conclusive. This parameter is based on $||H(f)||$ versus frequency, which involves a division of noisy data. However the conjectured form for H(f) in equation (8) can account for the shape of the data. Further work in the analysis of mixing in a variable length capillary bed is necessary to ascribe a physiological meaning to σ.

As the work reported here came to an end, the retinal image acquisition system and tracer injection techniques were improved. Controllable tracer injection pulses became possible, and with a higher pixel resolution and a wider field of view, dye dilution curves for any arteries and veins in the retinal circulatory system could be simultaneously obtained. The need for characterizing the entire retinal circulatory system is clear. The improvements in the data acquisition system and the results reported here show the potential for further retinal hemodynamic analysis. This would entail evolving further the models that were presented here and developing additional numerical techniques for estimating retinal blood volume and flow rates and the extent to which retinal capillary beds interact. To this point both experimental and numerical evidence

has been given to show that with the Television Ophthalmoscope the goal of obtaining reliable estimates of retinal hemodynamic parameters can be achieved.

The next step is the development of an interactive and dedicated computer system for dye dilution data analysis. With recent advances in microelectronics, this could be accomplished with a relatively small microcomputer system.

REFERENCES

[1] K.L. Zierler, "Circulation times and the theory of indicator-dilution methods for determining blood flow and volume. In: *Handbook of Physiology*, Section 2, Volume 7, American Physiology Society, 1962.

[2] J.S. Read, A.C. Petersen, B.H. McCormick and M.F. Goldberg, "The television ophthalmoscope/image processor: methods and applications," *Proceedings of Computers in Ophthalmology*, St. Louis, MO, IEEE, April 1979.

[3] Grodkins, F.S., "Basic concepts in the determination of vascular volumes by indicator-dilution methods," *Circulation Res.* V.X, pp. 429-446, 1962.

[4] R. Priemer, "Modeling and analysis of retinal dye dilution curves," Technical Report *TVL* 1.8.28, Department of Electrical Engineering and Computer Science, University of Illinois at Chicago. December 1979.

[5] R.B. Bird, W.E. Steward and E.N. Lightfoot, *Transport Phenomena*, John Wiley and Sons, Inc., New York, 1966.

[6] J.B. Hickman and R. Frayser, "A photographic method for measuring the mean retinal circulation time using fluorescein," *Investigative Ophthalmology*, 4, pp. 876-884, 1965.

[7] G.N. Wise, C.T. Dollery and P. Henkind, *The Retinal Circulation*, Harper and Row, New York, New York, 1971.

[8] C.J. Bulpitt and C.T. Dollery, "Estimation of retinal blood flow by measurement of the mean circulation time," *Cardiovascular Research* 4, pp. 406-412, 197.

[9] J.G. Cunha-Vaz and J.J.P. Lima, "Estimation of human retinal blood flow by slit-lamp fluorophotometry," I. Methodology and instrumentation *IRCS J. Med. Sci.*, 3, p. 576, 1975.

[10] N. Ashton, "Studies of the retinal capillaries in relation to diabetic and other retinopathies," *Brit. J. Ophthal.*, 47, pp. 521-538.

[11] J.G. Gunha-Vaz, J.R. Fonseca, J.R.F. DeAbreu and J.J.P. Lima, "Diabetic retinopathy: human and experimental studies," *Trans. Ophthal. Soc., U.K.* 92, pp. 111-124, 1972.

[12] E. Kohner, "Retinal blood flow in diabetes mellitis," in *Diabetic Retinopathy*, J.R. Lynn, W. B. Anyder and A. Vaiser (eds.),. Grune and Stratton, New York, p. 71, 1974.

[13] J.J.S. Cant (ed.), *Vision and Circulation*, Proc. of the Third William Mackenzie Memorial Symposium (1974), Henry Kimpton Publishers, London, England, 1976.